Self-Tuning Electrostatic Energy-Harvester IC

Erick O. Torres, *Graduate Student Member, IEEE*, and Gabriel A. Rincón-Mora, *Senior Member, IEEE*

***Abstract*—Miniature self-powered systems like wireless microsensors that rely only on easily exhaustible tiny in-package batteries suffer from short lifetimes. Harvesters, however, extend life by replenishing consumed energy with energy from the environment. The problem is harvesters generate considerably low power so producing a net gain with which to recharge a battery requires ultra low-energy circuits. This paper presents a 1.5 × 1.5 mm^2 0.7-µm BiCMOS self-tuning electrostatic energy-harvester IC that adapts to changing battery voltages (V_{BAT}) to produce usable power from vibrations across V_{BAT}'s entire operating range. The prototype holds C_{VAR}'s voltage so that kinetic energy in vibrations can generate and steer current into the battery when capacitance decreases. Unlike in [13], the inductor-based precharger that charges C_{VAR} to V_{BAT} adapts to a constantly shifting V_{BAT} target. Collectively, the precharger and its self-tuning reference, system monitors, and other control circuits draw sufficient power to operate, yet dissipate low enough energy to yield a net gain. Experimentally, the harvester IC generates 1.93, 2.43, and 3.89 nJ per vibration cycle at battery voltages 2.7, 3.5, and 4.2 V, which at 30 Hz produce 57.89, 73.02, and 116.55 nW. Accordingly, the system charges 1 µF from 2.7 to 4.2 V (a thin-film Li-Ion range) in 69 s and harnesses 47.9% more energy than with a fixed reference in the same time frame.**

***Index Terms*— Electrostatic harvester IC, vibrations, kinetic energy, microsensor, microsystem, harness ambient energy**

I. Electrostatic Energy Harvesting

THIN-FILM lithium-ion (Li-Ion) batteries [1] and miniature fuel cells [2] that power wireless microsensors and other self-powered microsystems only hold sufficient energy to sustain operations for short lifetimes [3]. In these cases, extracting energy from the surrounding environment [4]-[5] can extend life, if not indefinitely, substantially. Fortunately, kinetic energy in motion and vibrations [5]-[6] is abundant and reliable in a wide variety of applications. Harnessing this type of ambient energy with piezoelectric [7] and electromagnetic [8] materials, however, is challenging because these transducers are difficult and costly to integrate. Electrostatic harvesters, on the other hand, require vibration sensitive variable capacitors (C_{VAR}) that mainstream MEMS technologies can avail without the need for exotic and often expensive materials [5], [9]-[10].

In an electrostatic approach, vibrations work against C_{VAR}'s electrostatic force to separate its plates and decrease its capacitance. Because charge q_C is $C_{VAR}v_C$, holding q_C constant while C_{VAR} decreases raises v_C and, accordingly, C_{VAR}'s energy. Constraining q_C, however, induces v_C to increase up to 300 V, which exceeds the breakdown limits of low-cost semiconductor processes [11]. Alternatively, clamping v_C to battery voltage V_{BAT} is more benign and efficient because the charge vibrations generate flow directly to the battery as harvesting current i_{HARV} [12]. Although charging C_{VAR} to V_{BAT} increases the force against which vibrations work, typical Li-Ion, NiMH, NiCd, and Alkaline voltages (e.g., 0.9 – 4.2 V) are not expected to noticeably impede variations in C_{VAR}.

Manuscript received December 28, 2009. This work was supported by Texas Instruments Analog Fellowship Program.

The authors are with the Georgia Tech Analog, Power, and Energy IC Research Laboratory, School of Electrical and Computer Engineering, Georgia Institute of Technology, Atlanta, GA 30332-0250 USA (email: erick.torres@gatech.edu; rincon-mora@gatech.edu).

II. Battery-Constrained Electrostatic Harvester

To start, C_{VAR} requires charge to establish the electrostatic force against which vibrations work to separate the plates. For this reason, the battery must invest energy E_{INV} to precharge C_{VAR} to V_{BAT} when C_{VAR} is at C_{MAX}, as seen in Fig. 1, where E_{INV} is $0.5C_{MAX}V_{BAT}^2$. As vibrations decrease C_{VAR} to C_{MIN}, V_{BAT} clamps C_{VAR}, receives i_{HARV}, and gains harvesting energy E_{HARV} (i.e., $\Delta C_{VAR}V_{BAT}^2$) [12]-[13]. At C_{MIN}, C_{VAR} disconnects from V_{BAT} and C_{VAR}'s voltage resets to a lower value (as C_{VAR} increases to C_{MAX}), prompting another cycle to begin. As long as E_{HARV} exceeds E_{INV} and all other system losses E_{LOSS}, the battery gains energy E_{NET} (i.e., $E_{HARV} – E_{INV} – E_{LOSS}$).

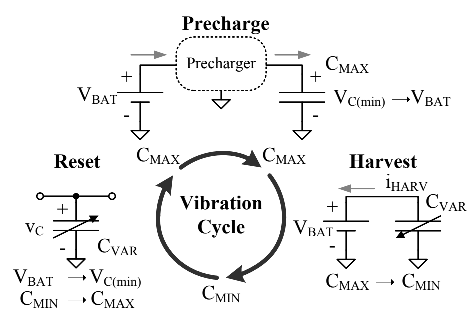

Fig. 1. Energy-harvesting phases: precharge, harvest, and reset [13].

To minimize losses and therefore yield a net energy gain, V_{BAT} precharges C_{VAR} with the quasi-lossless inductor-based precharger shown in Fig. 2 [13]. Switch MP_E initiates precharge by energizing inductor L and C_{VAR} from V_{BAT}. When L stores the energy necessary to finish precharging C_{VAR} to V_{BAT}, MP_E opens and MN_D closes, allowing L to de-energize into C_{VAR} until inductor current i_L is zero and v_C reaches V_{BAT}. At this point, MP_E and MN_D open and the system connects C_{VAR} to V_{BAT} to clamp and channel i_{HARV} through switch MP_H. Note that precharging C_{VAR} from 0 to V_{BAT} directly with MP_H is prohibitively lossy because MP_H conducts current while sustaining a higher voltage $V_{BAT} – v_C$. By transferring energy through L, neither transistor (MP_E or MN_D) sustains high terminal voltages while concurrently conducting i_L. And since the precharge process is significantly faster (at less than 250 ns) than vibrations (at roughly 1 – 100 Hz), the circuit perceives C_{VAR} as a constant near C_{MAX}.

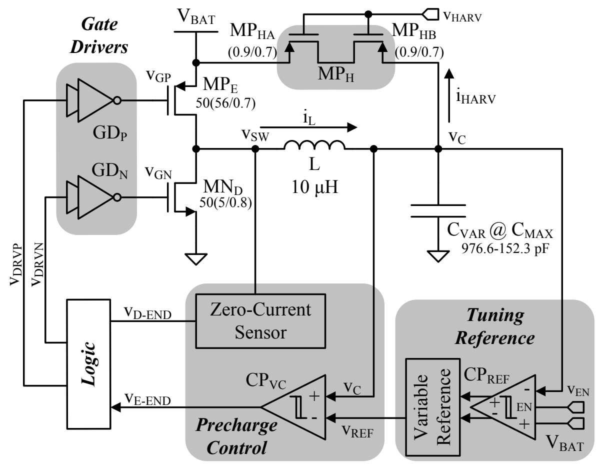

Fig. 2. Self-tuning precharger circuit (all dimensions are in µm).

To ensure the system invests sufficient energy E_{INV} to raise v_C to V_{BAT} during precharge, V_{BAT} should energize L and C_{VAR} for one-sixth of its natural resonant frequency, which corresponds to energizing L and C_{VAR} until v_C reaches $V_{BAT}/2$ [14]. In practice, however, losses increase the energy needed so v_C must rise to a higher voltage that reference v_{REF} sets when comparator CP_{VC} in Fig. 2 trips. E_{INV} and v_{REF} should also track V_{BAT} as i_{HARV} charges the battery to avoid under- or overcharging C_{VAR} about V_{BAT}, which would otherwise impress a higher voltage (and dissipate more power) across MP_H at the beginning of the harvesting phase. In other words, by tuning v_{REF} to V_{BAT}, the precharger invests the adequate amount of energy needed to charge C_{VAR} to V_{BAT}, irrespective of the battery's voltage and other circuit conditions. To this end, unlike in [13], the dynamic self-tuning precharger described in Section III, detailed in Section IV, and measured in Section V adjusts v_{REF} to ensure C_{VAR} precharges to V_{BAT}.

III. SELF-TUNING PRECHARGER

The proposed harvester regulates how much energy V_{BAT} invests in L and C_{VAR} by tuning (on a cycle-by-cycle basis) the precharger's energizing time t_E. After each precharge phase, comparator CP_{REF} in Figs. 2 and 3 compares v_C to V_{BAT} to determine whether L under- or overcharged C_{VAR}. If overcharged (i.e., $v_C > V_{BAT}$), CP_{REF} decreases v_{REF} to reduce t_E (and E_{INV}) for the subsequent vibration cycle. Conversely, v_{REF} increases if the precharger undercharges C_{VAR} below V_{BAT}. In steady state, the system tunes t_E to charge C_{VAR} to V_{BAT} accurately, which minimizes Ohmic losses across MP_H.

CP_{REF} in Fig. 3 compares V_{BAT} and v_C only while converging on a decision after each precharge phase, shutting off immediately after that. Current source I_{CH} and sink I_{DCH} pump or remove charge Δq_{REF} from on-chip reference capacitor C_{REF} to increase or decrease v_{REF} by a fixed amount (Δv_{REF}). In steady state, v_{REF} toggles between its two most optimal values (for a given V_{BAT}), changing in Δv_{REF} steps to correspondingly adjust the precharger's energizing time of the next cycle. When the system initializes, however, v_{REF} rises from ground one Δv_{REF} at a time so the harvester is unable to yield energy until v_{REF} is within a margin of its optimal state.

The system regulates v_C's final precharge voltage by tuning t_E with a feedback loop in discrete time. In other words, it operates only during a small fraction of vibration period to generate a v_{REF} setting for the next cycle. C_{REF} in Fig. 3 then holds that state for the remainder of the cycle. In this way, the loop dissipates power only for a small portion of the period. Including so much time for signals to settle introduces a dominant pole to the loop that decreases the loop gain to one at a frequency that is considerably lower than all other poles in the loop, which is why the circuit is stable. Note the feedback loop disappears (breaks) with a fixed reference because v_C resets and charges to a fixed preset value every cycle.

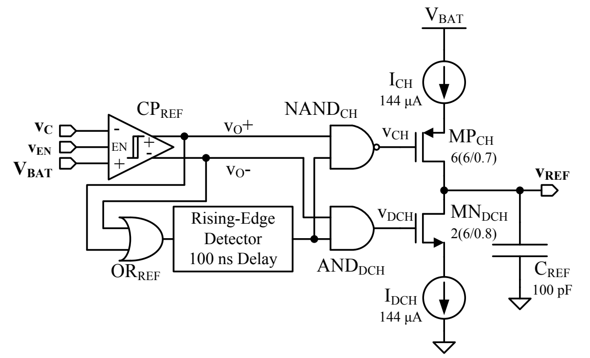

Fig. 3. Tuning reference circuit (all dimensions are in µm).

IV. INTEGRATED CIRCUIT DESIGN

System: The system integrates all blocks (including phase detection and control circuits) into one IC, with the exception of L, C_{VAR}, and bias current-setting resistors, which are off chip for experimental flexibility. CP_{REF}, which is at the core of the self-tuning loop, monitors v_C with preamplifier AMP_{PRE} and drives the programmable reference block with latch comparator CP_{LATCH}, as Fig. 4(a) shows. Based on CP_{REF}'s output, logic engages MP_{CH} or MN_{DCH} to charge or discharge C_{REF} through the designed delay that the rising edge-detector in Fig. 4(b) sets. After v_{REF} settles to its new state, switch MP_H closes to start the harvesting phase.

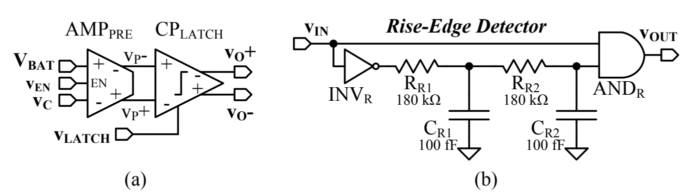

Fig. 4. (a) CP_{REF}'s preamplifier (AMP_{PRE}) and latching comparator (CP_{LATCH}) stages and (b) 100-ns delay rising-edge detection circuit.

Charge Pump: While CP_{REF}'s outputs v_O^+ or v_O^- determine whether to charge or discharge poly-poly capacitor C_{REF} with currents I_{CH} or I_{DCH}, the rising-edge detector in Fig. 4(b) sets for how long. When either v_O^+ or v_O^- output turns high, it triggers, through OR_{REF}, the rising-edge detector, which remains high for a designed 100-ns delay (t_{DLY}). Therefore, if v_O^+ transitions to a high state, for example, logic gate $NAND_{CH}$ trips and engages MP_{CH} until the delayed signal, also fed into $NAND_{CH}$, changes to a low state. Conversely, AND_{DCH} engages MN_{DCH} when v_O^- rises. The rise-edge detector's series RC network maintains the signal high for t_{DLY}, which means C_{REF} charges or discharges for approximately 100 ns. Note that a constant delay fixes C_{REF}'s charge variation ΔQ_{REF} to $I_{CH}t_{DLY}$, independent of C_{REF}, which only influences voltage change Δv_{REF} (i.e., $\Delta Q_{REF}/C_{REF}$). A local bias block that only operates during precharge generates I_{CH} and I_{DCH} so the precharger only dissipates quiescent power during a diminutive fraction of every vibration cycle.

Leakage currents in the circuit and printed circuit board (PCB), however, discharge C_{REF} when the precharger is off for about 33 ms (with 30-Hz vibrations). This means v_{REF} droops between sampling events and ΔQ_{REF} must therefore surpass leaked charge Q_{LEAK} (i.e., $I_{CH}t_{DLY} > I_{LEAK}T_{VIB}$). For this reason, while at steady state, CP_{REF} raises v_{REF} several steps for each time CP_{REF} decreases v_{REF}. While ΔQ_{REF} and Q_{LEAK} do not depend on C_{REF}, increasing C_{REF} mitigates (but does not resolve) the issue by reducing Δv_{REF}. Increasing I_{CH}, on the other hand, would cancel the effects of Q_{LEAK}, but only at the expense of greater energy losses (i.e., more charge).

Latch Comparator: After each precharge event, enabling signal v_{LATCH} closes MN_{EN} and opens $MP_{EN1\text{-}EN4}$ in Fig. 5 to engage CP_{LATCH} in Fig. 4 (and detailed in Fig. 5). The complementary outputs of buffer preamplifier AMP_{PRE} create a current imbalance in differential transistors MN_{11} and MN_{12} that triggers the positive feedback loop across $MN_{13\text{-}14}$ and $MP_{15\text{-}16}$ and drives complementary output inverters MN_{2A}-MP_{2A} and MN_{2B}-MP_{2B}. Once enabled, nodes v_{13} and v_{14} latch to supply or ground, ensuring the circuit remains in a zero-current state to reduce power [15]. The role of AMP_{PRE} is to (*i*) drive signals within CP_{LATCH}'s input common-mode range (ICMR), (*ii*) shunt switching noise that CP_{LATCH} couples back into v_{INL}^+ and v_{INL}^-, and (*iii*) increase CP_{LATCH}'s input overdrive (to accelerate its response) and dynamic range (to avoid inadvertent transitions) by amplifying the difference sensed in v_C and V_{BAT} before feeding them into CP_{LATCH}.

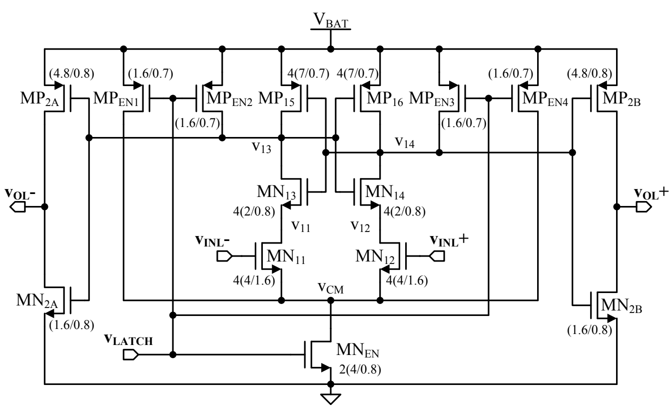

Fig. 5. Comparator CP_{REF}'s latch CP_{LATCH} (all dimensions are in μm).

Preamplifier: To fully accommodate v_C's range (from ground to above V_{BAT}) and amplify enough of V_{BAT} and v_C's difference for CP_{LATCH} to operate properly, AMP_{PRE} in Fig. 6 features complementary p- and n-type differential pairs MP_{2A}-MP_{2B} and MN_{4A}-MN_{4B}. Source followers MN_{1A}-MN_{1B} level-shift the inputs to help input pair MN_{4A}-MN_{4B} maintain enough dynamic range across resistor load R_{L1}-R_{L2} when v_C exceeds V_{BAT}. Architecturally, MN_{4A}-MN_{4B} feed currents directly to R_{L1}-R_{L2} while MP_{2A}-MP_{2B} fold theirs into the load through cascodes MN_{3A}-MN_{3B}. As a result, outputs v_p^+ and v_p^- swing between V_{BAT} and roughly 1 V below V_{BAT} (with 16 μA into 62.5 kΩ), which is sufficiently high to drive CP_{LATCH}'s input NMOS pair. Note that AMP_{PRE} derives its bias currents from the same local precharge bias generator as the charge pump, which the system only enables (with v_{EN}) for a small fraction of each vibration period to keep quiescent losses low.

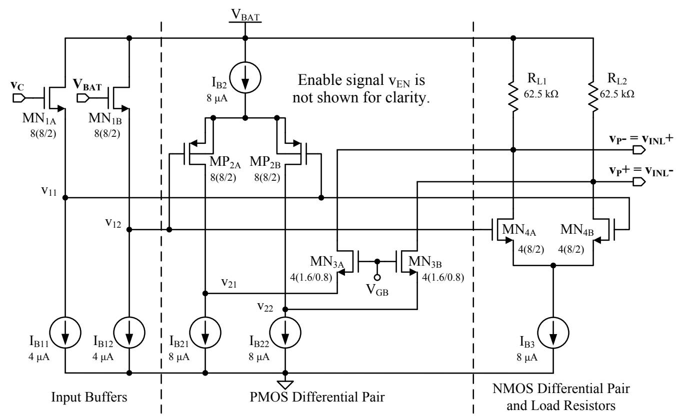

Fig. 6. Comparator CP_{REF}'s preamplifier AMP_{PRE} (all dimensions are in μm).

V. Experimental Validation

Prototype: The 1.5 × 1.5 mm^2 silicon die pictured in Fig. 7(a), which is encapsulated in a 32-pin plastic quad-flat package (PQFP), integrates the proposed self-tuning energy-harvesting system. The IC also includes test-mode logic and pin-out digital buffers and was tested with the PCB in Fig. 7(b). A 2 × 2-mm^3 10-μH Coilcraft inductor with a maximum equivalent series resistance (ESR) of 1 Ω served as precharge inductor L and the prototyped variable capacitor in [13] as C_{VAR}, which oscillates at 30 Hz between 991.2 and 156.8 pF when shaken by a Brüel & Kjær 4810 vibration source. v_{REF} was pinned out for testing purposes, but no electrostatic-discharge protection (ESD) was included to keep the large ESD circuit from leaking C_{REF}.

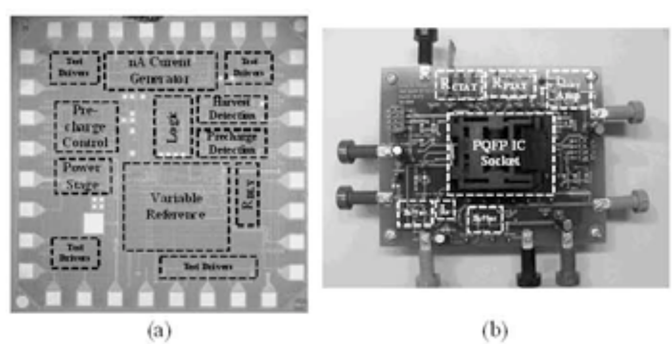

Fig. 7. (a) Die photograph of the 1.5 × 1.5 mm^2 energy harvester IC and (b) the printed-circuit board (PCB) used to experimentally test it.

Performance: As the experimental results from Fig. 8 show, C_{VAR} generates (on average) up to 505.3 nA (i_{HARV}) when shaken and clamped to a 3.5-V battery. MP_H conducts i_{HARV} into the battery, which when integrated over time, represents (with E_{HARV}) an average gain of 10.1 nJ/cycle. At the end of each harvesting phase, MP_H disengages and i_{HARV} drops to zero, and the reset phase follows with v_C gradually dropping. The harvesting detection circuit, which is active through the harvesting phase (for roughly 17.77 ms/cycle on average), consumes a (measured) quiescent current I_Q of 2.63 – 3.75 nA, resulting in 209.76 pJ/cycle of used energy. Similarly, the precharge detector draws a measured I_Q of 1.80 – 3.69 nA for the duration of the reset phase (for approximately 15.56 ms/cycle on average), resulting in roughly 141.06 pJ/cycle. A nanoampere current generator, which biases both detection blocks, remains operational through the entire period (for 33.33 ms, on average, which corresponds to 30-Hz vibrations), sinks 2.48 – 2.96 nA from the 3.5-V supply, and uses an average of 320.34 pJ/cycle. Note: A 100-V/V LTC1100 instrumentation amplifier (with less than 0.075% of gain error and 10 µV of input offset) measures i_{HARV} by sensing the voltage drop across a series resistance R_{HARV} (100 kΩ) [13].

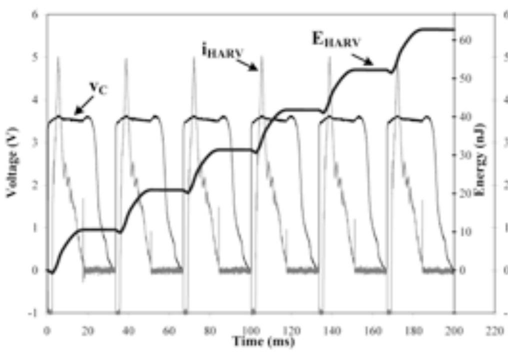

Fig. 8. Experimental measurements showing variable capacitor voltage v_C, harvesting current i_{HARV}, and extrapolated energy gain E_{HARV}.

The system invests the necessary energy from the battery (through L) to charge C_{VAR} to its 3.5-V target during every precharge phase. The self-tuning precharger energized L and C_{VAR} (on average) for about 134.2 ns, producing a peak inductor current of 24.15 mA. L then de-energized into C_{VAR} in 92.55 ns, resulting in an average invested energy of 6.72 nJ/cycle. The precharge control circuit, which includes the zero-current sensor and the comparator that sets energizing time t_E, only operate during the energize and de-energize steps and use 44.19 pJ/cycle. The precharge bias generator powers when C_{VAR} reaches C_{MAX} to become functional after roughly 245.25 ns, after which the energize/de-energize sequence initiates. As a result, the generator uses 31.82 pJ/cycle, totaling the energy lost in the control circuit to 76.01 pJ/cycle.

Reference voltage v_{REF}, which sets v_C's energizing time t_E, adjusts after each precharge phase and varies between 2 and 2.5 V when tested at 3.5 V (Fig. 9). On average, the system raises v_{REF} by 189.50 mV and decreases it by 164.38 mV by charging or discharging C_{REF} (100 pF). An average of 376.33 pA leaks C_{REF} to decrease v_{REF} by 125.43 mV every cycle, limiting the rise in v_{REF} to 64.07 mV and increasing the drops to 289.81 mV. For this reason, v_{REF} increases (on average) 3.48 times for every time it decreases. Note, however, the off-chip test buffer used to measure v_{REF} leaked considerable charge from C_{REF}. On average, though, each charge event in C_{REF} uses 48.41 pJ/cycle, and the charge pump and CP_{REF} power with the precharge comparators to dissipate 33.26 – 35.43 µA and 39.79 – 44.98 µA for 489.95 ns and use 57.11 pJ/cycle and 70.29 pJ/cycle, respectively. When the system first powers (during startup, as shown in Fig. 10), v_{REF} charges incrementally (each cycle) from ground until it reaches steady state after about 25.63 cycles (on average).

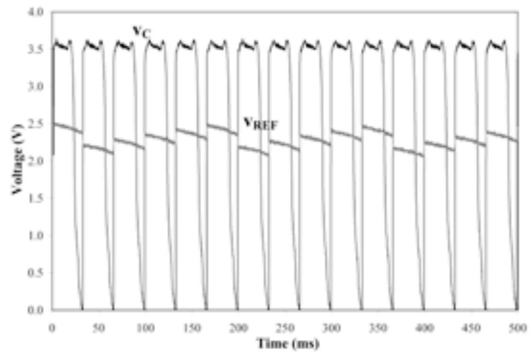

Fig. 9. Experimental waveforms showing variable capacitor voltage v_C and variable reference voltage v_{REF}.

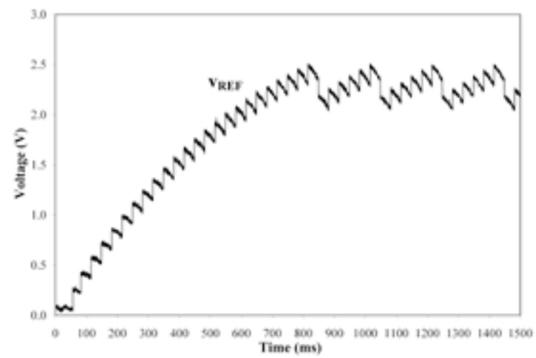

Fig. 10. Prototyped variable v_{REF} during startup and through steady state.

Ultimately, the total energy the system drew from vibrations in C_{VAR} exceeded all losses, producing a net gain of 2.434 nJ/cycle for a 3.5-V battery, which is equivalent to 73.02 nW at 30 Hz. The system also produced gains of 1.930 and 3.885 nJ/cycle at 2.7 and 4.2 V, which represents the operating range of typical Li Ions, for 57.89 and 116.55 nW at 30 Hz, as summarized in Table I. Note that charging an actual battery is impractical during testing because the large capacities that commercial batteries feature lead to months long charge times. Instead, the 1-µF ceramic capacitor C_{BAT} the harvester charged from 2.7 to 4.2 V in Fig. 11 illustrates the nominal charging profile of a microscale (low-capacity) battery.

Across 8 samples and 51 measurements, the harvester charged C_{BAT} from 2.7 to 4.2 V (with 5.175 µJ) in 68.84 s (on average). This represents an average of 75.18 nW for the entire voltage range. Tuning reference v_{REF} increased from 1.5 to 2.7 V, self-adjusting to V_{BAT}. A fixed 2.3-V reference, which is the average value of v_{REF} for a 3.5-V battery, results in less gain, extending C_{BAT}'s charge time (Fig. 11). In other words, the harvester only generates 3.499 µJ to charge C_{BAT} to 3.78 V in the same time the proposed circuit charged C_{BAT} to 4.2 V. Note that the variable reference block is disabled during this latter experiment to avoid dissipating the power a fixed reference would not. In the end, the self-tuning v_{REF} loop leads to a 47.9% improvement (even without considering the losses an internal fixed reference circuit would incur).

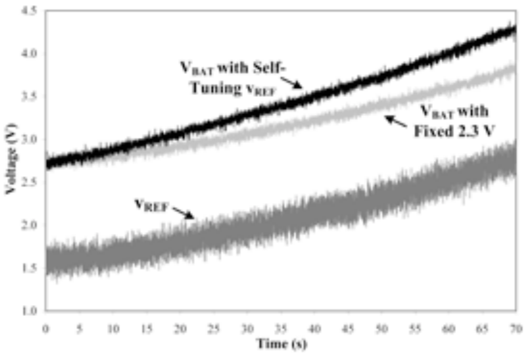

Fig. 11. Experimental voltage profile of a 1-μF capacitor when charged with the energy harvester IC with the proposed self-tuning v_{REF} and a fixed 2.3-V reference.

Discussion: In charging a ceramic capacitor, the system circumvents the need for battery protection, which means a practical implementation requires additional energy to protect a thin-film Li Ion, for example. This extra energy, however, need not be substantial when duty-cycling the circuit to engage only for a fraction of the vibration cycle with subthreshold currents. As already mentioned, v_{REF} is also prone to leakages. A counter and a conventional digital-to-analog converter (DAC) would avoid those effects, but at the expense of more silicon area. v_{REF}'s accuracy and the energy investment it tunes would also improve if its incremental variation Δv_{REF} were proportional to $v_C - V_{BAT}$ (instead of being fixed, as is the case in the system presented). Notwithstanding, the prototyped implementation validates and demonstrates the value of self-tuning the system to adapt to and compensate for a changing (i.e., charging and discharging) battery voltage, irrespective of circuit non-idealities like losses, delays, offsets, etc.

VI. Conclusions

The presented IC gains 1.930, 2.434, and 3.885 nJ/cycle from 30-Hz vibrations at battery voltages 2.7, 3.5, and 4.2 V, respectively, and charges 1 μF from 2.7 to 4.2 V (i.e., a thin-film Li-Ion range) in 68.84 s. The system did this by automatically tuning the energizing time (t_E) of an energy-transfer inductor (L) in finite and constant steps (as determined by Δv_{REF}) to precondition and precharge C_{VAR} to V_{BAT} every cycle, irrespective of V_{BAT}. In this way, the system adjusts the energy invested to what is needed, no more and no less. This type of correcting loop is especially critical in energy-constrained microscale harvesters for extending the operational life of, for example, self-powered wireless microsensors.

Table I. Self-Tuning Harvester IC Performance

Die Information		1.5 × 1.5 mm² 0.7-μm BiCMOS IC		
V_{BAT} Range		2.7 V	3.5 V	4.2 V
CP_{REF}	$I_{Q.AVG}$	39.70 μA	42.34 μA	44.18 μA
	v_O^+ Delay	10.54 ns	8.19 ns	7.47 ns
	v_O^- Delay	10.55 ns	8.36 ns	7.46 ns
Charge Pump	$I_{Q.AVG}$	31.09 μA	33.99 μA	35.37 μA
Time ON	$t_{ON.AVG}$	512.9 ns	489.4 ns	478.5 ns
Variable v_{REF} (Averages)	$v_{REF.MAX}$	1.930 V	2.496 V	3.076 V
	$v_{REF.MIN}$	1.535 V	2.046 V	2.553 V
	$\Delta v_{REF.UP}$	172.2 mV	189.5 mV	198.6 mV
	$\Delta v_{REF.DOWN}$	–159.4 mV	–164.4 mV	–178.8 mV
	$\Delta v_{REF.LEAK}$	–96.3 mV	–125.4 mV	–163.2 mV
Measured Energy (nJ/cycle)				
Energy Harvested E_{HARV}		+6.842	+10.073	+14.335
Precharge Investment E_{INV}		–4.206	–6.717	–9.325
v_{REF} Losses		–0.127	–0.176	–0.221
Control/Detection Losses		–0.579	–0.747	–0.905
Net Energy Gain E_{NET}		***+1.930 nJ***	***+2.434 nJ***	***+3.885 nJ***
Power Generated at 30 Hz		***57.89 nW***	***73.02 nW***	***116.55 nW***

References

[1] N.J. Dudney, "Thin film micro-batteries," The Electrochemical Society's Interface, vol. 17, no. 3, pp. 44-48, Fall 2008.

[2] J. Li, *et al*, "Microfabricated fuel cell with composite glass/nafion proton exchange membrane," *Journal of the Electrochemical Society*, vol. 153, no. 2, pp. A343-A347, Feb. 2006.

[3] D. Puccinelli and M. Haenggi, "Wireless sensor networks: applications and challenges of ubiquitous sensing," *IEEE Circuits and Systems Magazine*, vol. 3, no. 3, pp. 19-29, 2005.

[4] E.O. Torres and G.A. Rincón-Mora, "Energy-harvesting system-in-package (SiP) microsystem," *ASCE Journal of Energy Engineering,* vol. 134, no. 4, pp.121-129, Dec. 2008.

[5] S. Roundy, P.K. Wright, and J.M. Rabaey, *Energy Scavenging for Wireless Sensor Networks with Special Focus on Vibrations*, 1st ed., Massachusetts: Kluwer Academic Publishers, 2004.

[6] P.D. Mitcheson, *et al*, "Energy harvesting from human and machine motion for wireless electronic devices," *Proceedings of the IEEE*, vol. 96, no. 9, pp. 1457-1486, Sept. 2008.

[7] S.R. Anton and H.A. Sodano, "A review of power harvesting using piezoelectric materials (2003-2006)," *Smart Materials and Structures*, vol. 16, no. 3, pp. R1-R21, June 2007.

[8] S.P. Beeby, *et al*, "A micro electromagnetic generator for vibration energy harvesting," *Journal of Micromechanics and Microengineering*, vol. 17, pp. 1257-1265, July 2007.

[9] S. Meninger, *et al*, "Vibration-to-electric energy conversion," *IEEE Transactions on Very Large Scale Integration (VLSI) Systems*, vol. 9, no. 1, pp. 64-76, Feb. 2001.

[10] B.C. Yen and J.H. Lang, "A variable-capacitance vibration-to-electric energy harvester," *IEEE Transactions on Circuits and Systems I*, vol. 53, no. 2, pp. 288-295, Feb. 2006.

[11] B.H. Stark and T.C. Green "Comparison of SOI power device structures in power converters for high-voltage, low-charge electrostatic microgenerators," *IEEE Transactions on Electron Devices*, vol. 52, no. 7, pp. 1640-1648, July 2005.

[12] E.O. Torres and G.A. Rincón-Mora, "Electrostatic energy-harvesting and battery-charging CMOS system prototype," *IEEE Transactions on Circuits and Systems I*, vol. 56, no. 9, pp. 1938-1948, Sept. 2009.

[13] E.O. Torres and G.A. Rincón-Mora, "A 0.7-μm BiCMOS electrostatic energy-harvesting system IC," *IEEE Journal of Solid-State Circuits*, vol. 45, no. 2, pp. 483-496, Feb. 2010.

[14] E.O. Torres and G.A. Rincón-Mora, "Energy budget and high-gain strategies for voltage-constrained electrostatic harvesters," *Proc. IEEE International Symposium on Circuits and Systems (ISCAS)*, pp. 1101-1104, May 2009.

[15] P.M. Figueiredo and J.C. Vital, "Kickback noise reduction techniques for CMOS latched comparators," *IEEE Transactions on Circuits and Systems II*, vol. 53, no. 7, pp. 541-545, July 2006.